Journal of Solid State Chemistry **143,** 33–40 (1999)
Article ID jssc.1998.8062, available online at http://www.idealibrary.com on IDEAL®

A New Niobium Tungsten Oxide as a Result of an *in Situ* Reaction in a Gas Reaction Cell Microscope

M. J. Sayagués[1] and J. L. Hutchison

Department of Materials, University of Oxford, Parks Road, Oxford OX1-3PH, United Kingdom

and

F. Krumeich

Laboratory of Inorganic Chemistry, ETH Zürich, CH-8093 Zürich, Switzerland

Received May 5, 1998; in revised form October 9, 1998; accepted October 9, 1998

$Nb_7W_{10}O_{47}$ was heated by an electron beam in a gas atmosphere (O_2, He, or H_2) of the gas reaction cell installed in a JEOL 4000 EX high-resolution transmission electron microscope (HRTEM). This treatment generated a new niobium tungsten oxide (Nb, W)$_{12}O_{32}$, crystallizing in a $\sqrt{2a} \times \sqrt{2a}$ superstructure of the tetragonal tungsten bronze (TTB) type. While the TTB substructure remains unaltered by this reaction, the proportion of pentagonal tunnels occupied with metal–oxygen strings has increased. The simultaneous occupation of all four pentagonal tunnels around a central square of octahedra is the characteristic structural feature of (Nb, W)$_{12}O_{32}$. This arrangement is observed here for the first time in the ternary system Nb/W/O. During the reaction, a part of the tungsten oxide is etched away and condenses as small particles near the irradiated crystallite. © 1999 Academic Press

1. INTRODUCTION

The combination of a high-resolution transmission electron microscope (HRTEM) with an *in situ* gas reaction cell (GRC) (1) provides an unique tool for the study of solid–gas reactions at the atomic level (2–4). In particular, the structural changes of nonstoichiometric niobium oxides NbO_x ($2.0 < x \leq 2.5$) caused by oxidation with O_2 or by reduction with H_2 have been successfully explored by this technique (2). These NbO_x phases crystallize in the so-called block structures. These structures are derived from the ReO_3 type, which consists of a cubic arrangement of corner-sharing octahedra by crystallographic shear in two orthogonal planes (5).

The tetragonal tungsten bronze (TTB) type represents another ReO_3-related structure (6). Tunnels of different shape appear inside a framework of corner-sharing MO_6 octahedra. The incorporation of metal atoms into these tunnels implies a reduction compared to WO_3, e.g., in the prototype K_xWO_3 ($x = 0.475$: $a = 1.2285$, $c = 0.3833$ nm (7)), which gives the name to this structure type. This structure principle allows to accommodate varying oxygen/metal ($O/\Sigma M$) ratios in a wide range. In TTB-type niobium tungsten oxides, metal–oxygen (MO) strings fill up some of the pentagonal tunnels (PTs) in such a way that a pentagonal bipyramidal coordination results for the cations in the tunnels. In connection with the five adjacent MO_6 octahedra, the structural element designated as a pentagonal column (PC, for short) is formed (8). In $Nb_8W_9O_{47}$ (cf. Fig. 8), one-third of the PTs are occupied in a systematic way so that a threefold TTB superstructure results (9). Two PCs are connected by the so-called diamond link (10) and thereby form PC pairs. A solid solution series $Nb_{8-n}W_{9+n}O_{47}$ ($0 < n \leq 5$), which crystallizes also with this structure, contains an amount of cations with lower valence (11). The oxidation of these phases leads to dramatic structural changes including a variety of new structural elements, which have been characterized by HRTEM (12, 13).

These interesting results have initiated the investigations presented in this paper. The heating of $Nb_7W_{10}O_{47}$ ($n = 1$ of the series $Nb_{8-n}W_{9+n}O_{47}$, $a = 1.222$, $b = 3.651$, $c = 0.394$ nm (11)) by an electron beam (under gas) in the GRC surprisingly generates a new niobium tungsten oxide, discovered and characterized by TEM methods.

2. EXPERIMENTAL

The synthesis of the starting material $Nb_7W_{10}O_{47}$ has been described elsewhere (11). The experimental microscopy

[1] To whom correspondence should be addressed at Instituto de Ciencia de Materiales de Sevilla CSIC c/Américo Vespucio, s/n, 41092, Sevilla, Spain.

0022-4596/99 $30.00

study has been carried out as follows:

Samples were prepared by dispersing a suspension of the powder in acetone onto a holey carbon film supported by a copper finder grid. The images were recorded between 300,000 × and 800,000 × at close to Scherzer focus. The image contrast was compared with simulated images (EMS program (14)). A finder grid (showing marks and codes in the grid squares to allow to localize the same area in different microscopes) was used for the purpose of treating and analyzing the same crystallite in three different microscopes.

1. Gas reaction cell (GRC) microscope (1). The GRC is based on a standard SAP40 polepiece, which is vacuum-sealed into the objective lens. A differentially pumped system was constructed with a number of extra apertures, which are sealed into the upper and lower polepieces, and a pumping line mounted in the polepiece spacer ring. That system allows a minimum vapor pressure of, e.g., 1–20 mbar around the sample, while it preserves a vacuum of less than 10^{-6} mbar in the electron gun. The cell is mounted completely within the polepiece, thus facilitating easy insertion (or removal) in the microscope column. The GRC is inserted in a JEOL JEM 4000EX microscope being operated at 400 kV with a LaB_6 filament and a side entry configuration ($\pm 45^\circ$ double tilt specimen holder).

The point resolution in such a microscope is about 0.26 nm in vacuum with a lattice resolution better than 0.21 nm; with the crystal under a gas environment, the point resolution (about 0.3 nm) will be restricted for obvious reasons.

Suitable crystallites were located with the cell under vacuum and oriented in the [001] zone axis. Later in the experiment, O_2, He, or H_2 was introduced into the specimen area and the focused electron beam was used (by changing or even removing the condenser aperture) to heat locally the crystal fragment.

2. HRTEM microscope. A JEOL JEM 4000EX (II), operating at 400 kV with a LaB_6 filament, is equipped with a top entry goniometer ($\pm 20^\circ$ tilt specimen holder). The same crystals treated in the GRC could be located and again oriented into the [001] zone axis. The point resolution in this microscope is about 0.16 nm, which allows us to be more accurate in resolving structural changes.

3. Analytical HRTEM. A JEOL 2010 microscope with an energy dispersive X-ray analysis system (EDX) is used to analyze the composition of the crystal before and after reaction. This system is equipped with a LINK system "Pentafet" windowless detector. The analysis was performed using a 3 nm diameter probe.

3. RESULTS AND DISCUSSION

3.1. Electron Microscopy of $Nb_7W_{10}O_{47}$ and the Reaction Products

Figure 1a presents the HRTEM micrograph along [001] of a crystal fragment (designated as crystal **A** in the following) of the starting material $Nb_7W_{10}O_{47}$. This image was recorded from a thin crystal region at close to the Scherzer defocus of the instrument so that the positions of the heavy atoms are recognizable a dark contrasts (15). This interpretation is confirmed by the simulation (inset in Fig. 1a). The threefold TTB superstructure is perfectly ordered in this area. The corresponding electron diffraction (ED) pattern (Fig. 1b) reveals the reflections of the threefold superstructure along an b^* axis of the TTB substructure.

The purpose of the first experiment was to attempt an *in situ* oxidation of the $Nb_7W_{10}O_{47}$ sample. Therefore, crystal A was treated in the GRC microscope under 15 mbar oxygen pressure. The beam was used as the heating device; the condenser apertures were removed in order to enhance the intensity of the electron beam. After an irradiation for 10 min, a HRTEM image and the corresponding ED pattern were recorded (Figs. 2a and 2b, respectively). A remarkable change has occurred as can be easily seen in the electron diffraction patterns: The reflections of the threefold TTB superstructure have vanished and new reflections in the center of the TTB reflections appear. The development of a different structure can be easily seen on the crystal edge (Fig. 2a). The gas cell was then flashed out and the gas was changed to H_2 in order to check if the reaction was reversible. However, no change could be observed after a treatment for 10 min under the electron beam.

Another three experiments were carried out to discern the structural transformation conditions exactly: one using He and another using H_2 (in both cases, a crystal fragment was heated with the electron beam) and the third without any gas (only heating with the electron beam). Surprisingly, the experiments using He and H_2 *produced the same structural transformation observed when oxygen was introduced*. Also remarkably, the last experiment under vacuum did not lead to any structural changes.

While for many structures the point resolution in the GRC microscope is sufficient to discern the structural changes during and after the gas reaction, the atomic details of the new structure formed in these experiments are not fully resolved. Thus, it was necessary to use a higher resolution microscope and study the transformed crystal A *ex situ*. The results obtained from a JEOL 4000 EX HREM are shown in Fig. 3, in which the new structure can be clearly seen. Although the basic TTB structure has been maintained, some rearrangements of the filled and empty PTs have occurred. Small crystalline particles around the treated crystal were also formed (Fig. 4). The significance of those is discussed below.

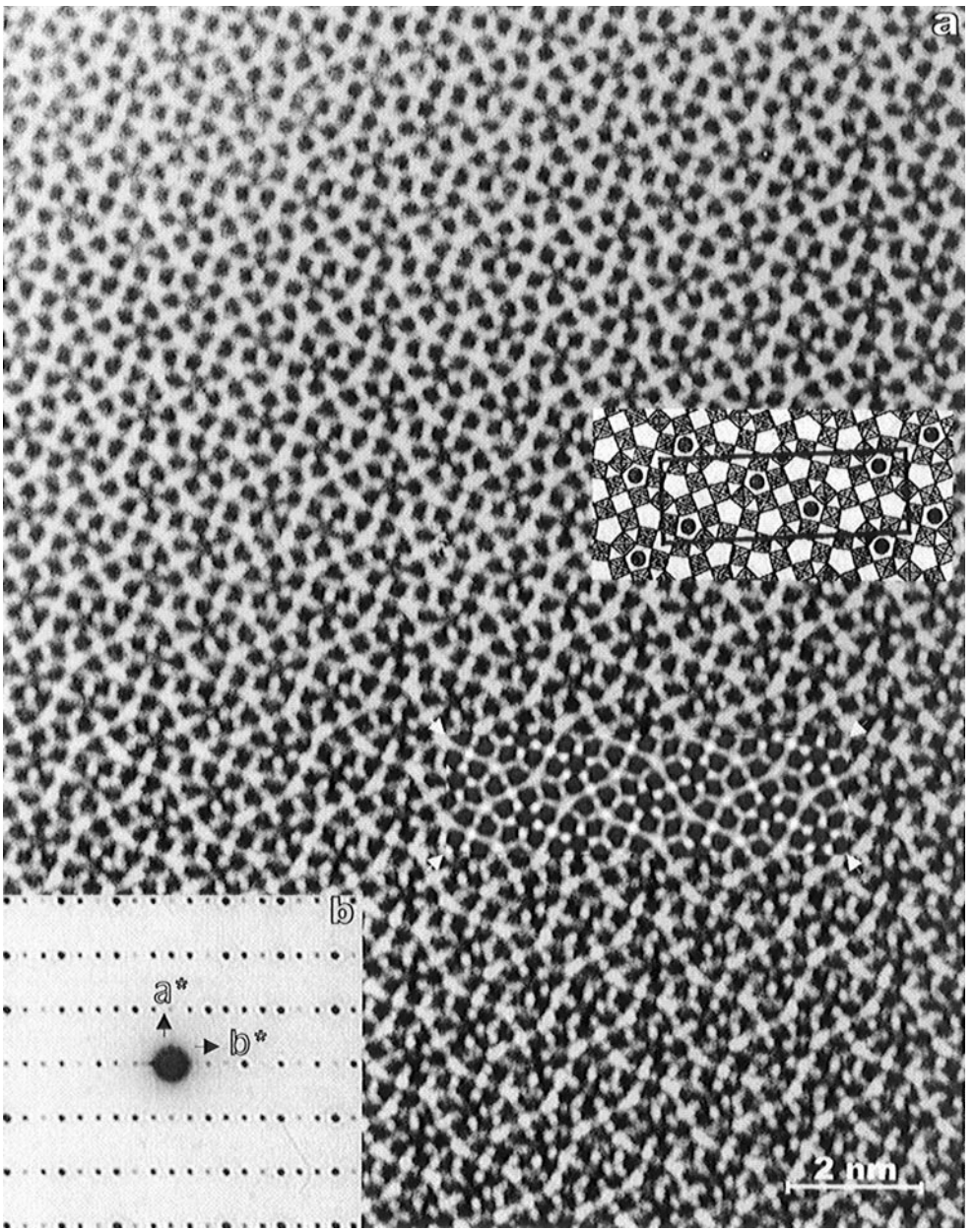

FIG. 1. (a) Micrograph of $Nb_7W_{10}O_{47}$ (crystal A) along [001] taken in the HRTEM microscope. The insets show a matched simulated image ($V_{acc} = 400$ kV, $C_s = 0.9$ mm, $f = -20$ nm, $\tau = 3.9$ nm) and the structural model. (b) Corresponding ED pattern.

Crystal A was analyzed with EDX before and after treatment in order to detect the compositional variations. Figure 5a shows the spectrum of $Nb_7W_{10}O_{47}$ and Fig. 5b the corresponding spectrum from the reaction product. It is obvious that the Nb/W ratio after treatment in the GRC has *increased* substantially compared with that of the starting material (with Nb/W = 7 : 10). Another spectrum (Fig. 5c) was taken from the small crystalline particles in the surrounding area (Fig. 4), and it corresponds to tungsten oxide. A fully quantitative analysis of Nb/W ratio of the new structure was impeded by additional particles located on the observed crystal fragment.

3.2. Description of the Structural Transformation

The TTB-type reflections are present in all ED patterns obtained before, during, and after the transformation (Fig. 6). This observation indicates that the TTB substructure is not involved into the structural changes induced by the irradiation under gas. On the other hand, the

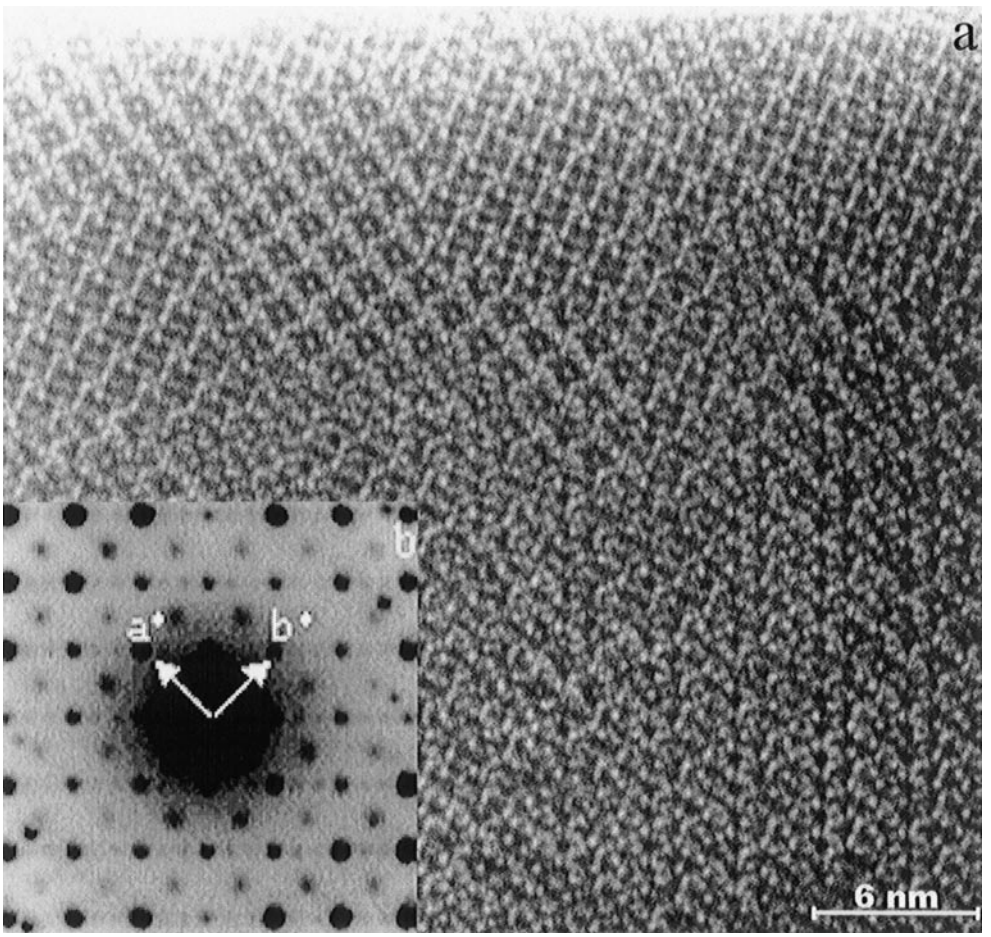

FIG. 2. (1) High-resolution image (crystal A) along [001] after 10 min in the GRC microscope under 15 mbar of oxygen. (b) Corresponding ED pattern of the region near the crystal edge.

superstructure reflections of the original threefold TTB superstructure vanish while new spots at $\{\frac{1}{2}\frac{1}{2}0\}_{\mathrm{TTB}}$ appear in the course of the experiments. This fact is due to the generation of a new $\sqrt{2}a_{\mathrm{TTB}} \times \sqrt{2}a_{\mathrm{TTB}}$ superstructure, with the lattice parameters being $a = b = 1.73$ nm. The length of the c-axis has not been determined experimentally in the course of this study, but it is well known that in this type of structure the polyhedra are linked by corner-sharing along this direction. Therefore, the translation period of this short crystallographic axis corresponds to the diagonal of such a polyhedron, which is about 0.39 nm.

The results of the *in situ* GRC investigations (Fig. 2a) provide more information about the structural changes during the process. The new structure motif appears as a bright dot, which is surrounded by a dark contrast, inside a square of bright dots. Microdomains consisting of these units appear in two distinct orientations. The structural details are revealed by HRTEM images, which have been obtained after the reaction in another microscope, which allows to resolve the positions of the metal atoms (Fig. 3). As we already know from the electronic diffraction patterns, the TTB substructure is still perfectly ordered. Furthermore, the arrangement of the PCs is quite regular in large domains: all four PTs adjacent to a central square of octahedra, i.e., all PTs of a TTB subcell, are occupied with M–O strings. In the HRTEM image, the PCs can be seen as a pentagon of dark dots, which has a dark dot in its center, whereas empty PTs appear as a pentagon of dark dots surrounding a bright one in the middle. The eight PTs in the adjacent TTB framework remain all empty. The positions of the metal atoms are determined from Fig. 3 and are listed in Table 1. Image simulations have been performed using these data. The good agreement between observed and calculated image contrast (Fig. 7) supports the structural model. The corresponding structural model is presented in Fig. 8. Of course, the oxygen atoms are not distinguishable in the HRTEM image; reasonable O positions have been estimated from a comparison with the TTB structure. The unit cell contains

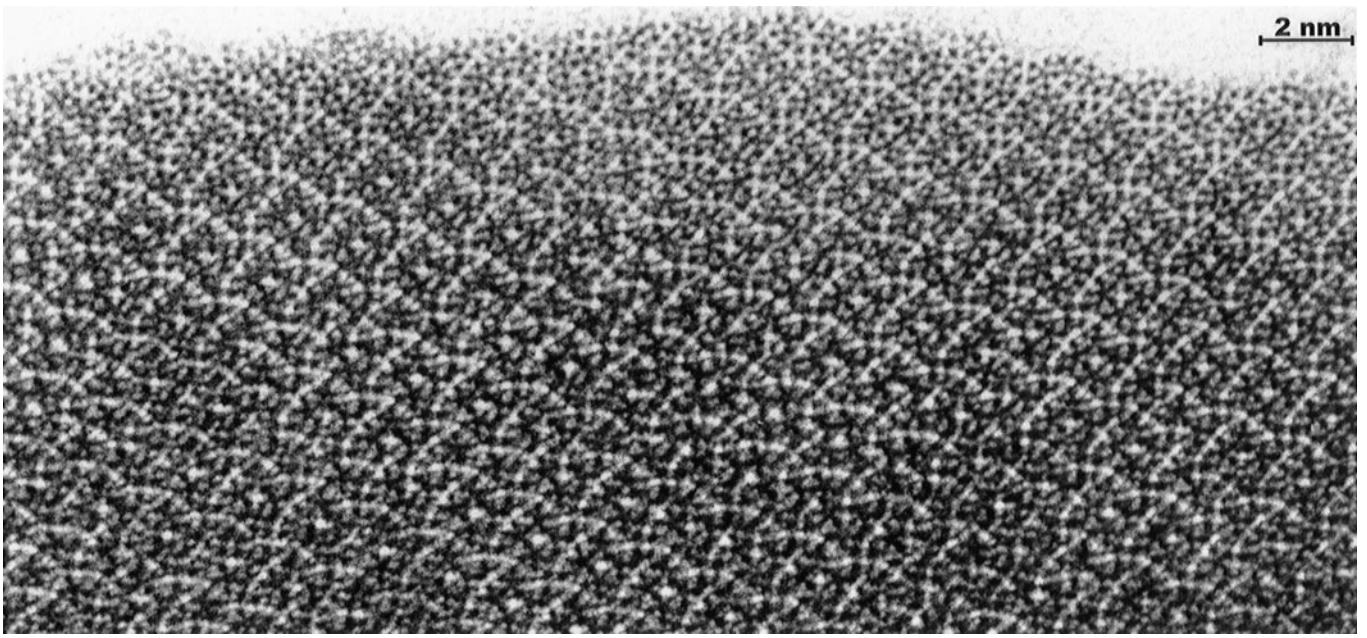

FIG. 3. Micrograph from crystal A along [001] after treatment in the GRC microscope (taken in the HRTEM microscope).

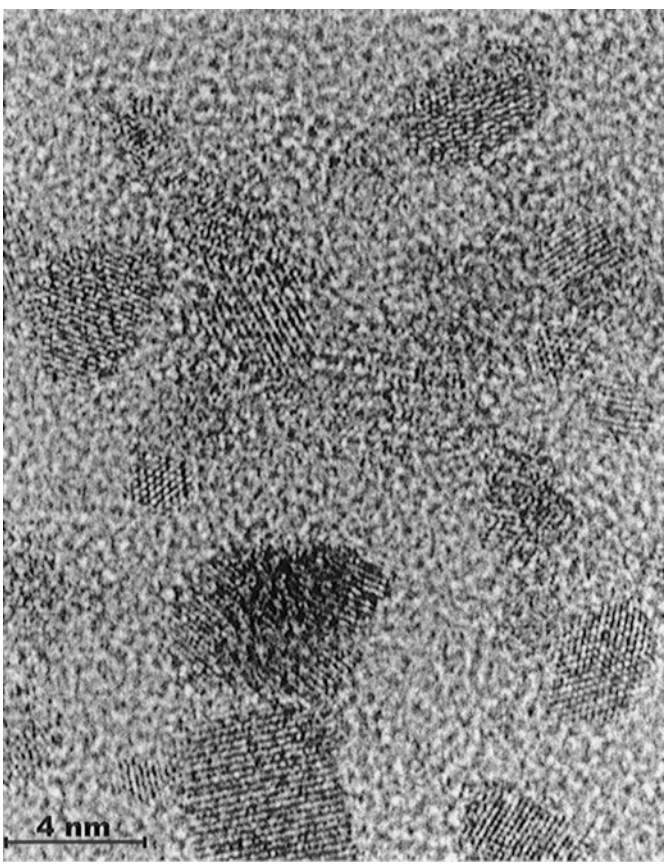

FIG. 4. Image of small particles found in the surrounding of the A crystal (taken in the HRTEM microscope). The particles were identified as tungsten oxide by EDX.

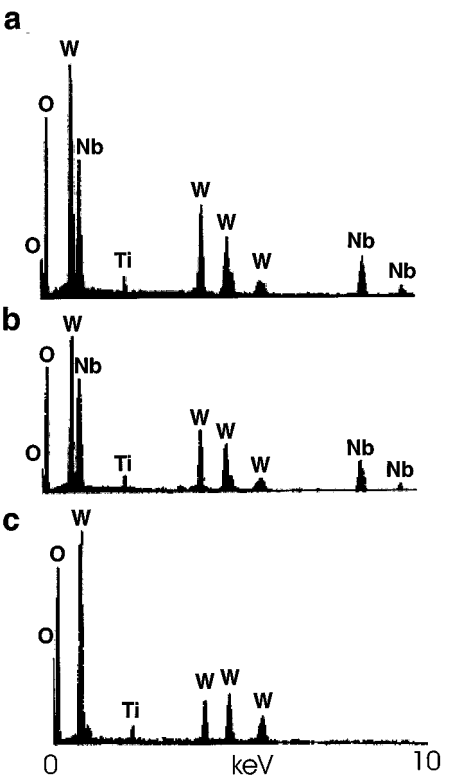

FIG. 5. EDX spectra of: (a) $Nb_7W_{10}O_{47}$ crystal, (b) the new structure formed after reaction in the GRC, and (c) small crystalline particle area (WO_{3-x}).

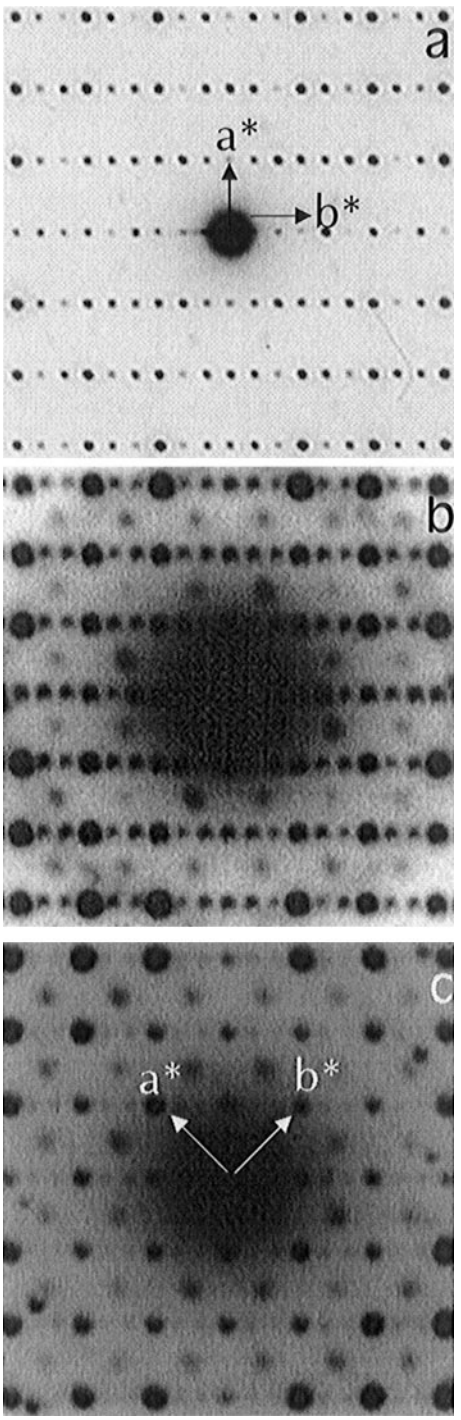

FIG. 6. Observed ED patterns along [001] of A crystallite: (a) before the transformation, (b) during the transformation, and (c) after the transformation.

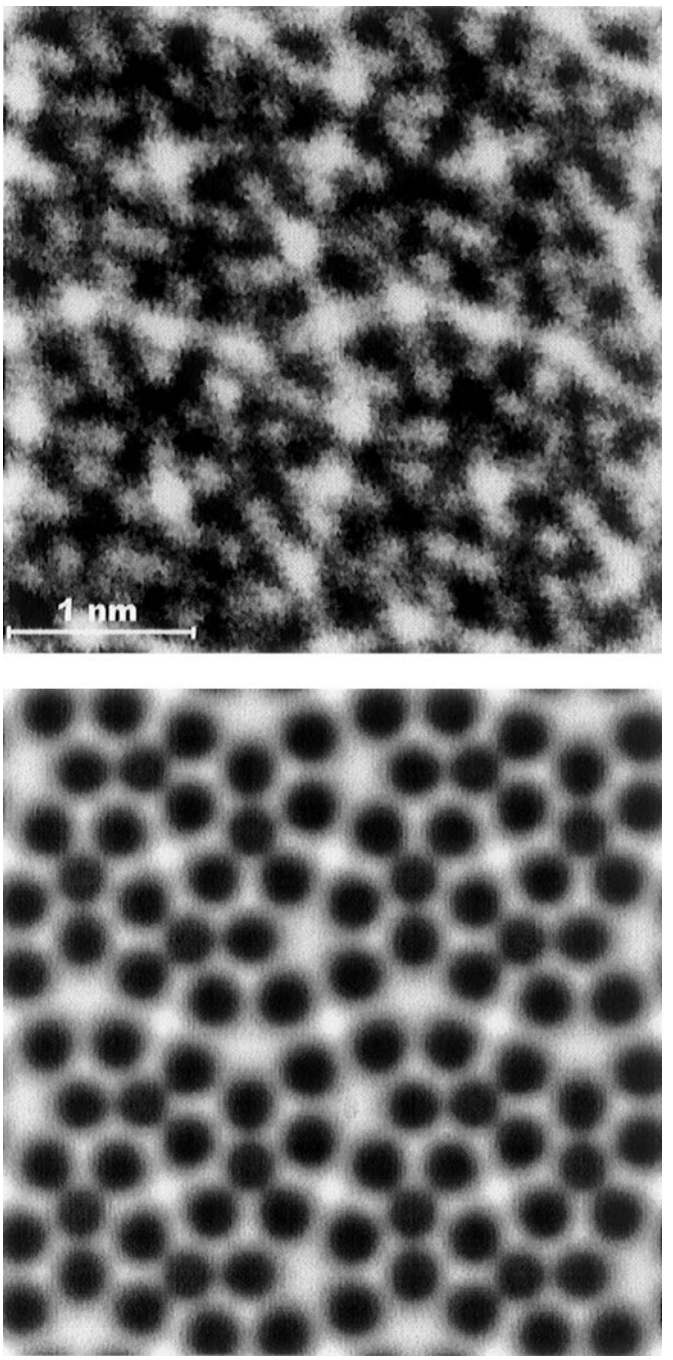

FIG. 7. Observed and calculated HRTEM images of 2×2 unit cells of $(Nb, W)_{12}O_{32}$. Parameters of the microscope and the crystal thickness for the simulation: $V_{acc} = 400$ kV, $C_s = 0.9$ mm, $f = -50$ nm, $\tau = 7.8$ nm.

two TTB subcells of composition $M_{10}O_{30}$ (M = Nb, W). Four of the eight PTs are occupied so that the composition of the unit cell becomes $(MO)_4(M_{10}O_{30})_2$, i.e., $(Nb, W)_{12}O_{32}$ and $(Nb, W)_6O_{12}$ for the asymmetric unit. Thus, the oxygen–metal ratio ($O/\sum M = 2.667$) is *lowered* compared to that of the starting material $Nb_7W_{10}O_{47}$ ($(MO)_4(M_{10}O_{30})_3$, $O/\sum M = 2.765$). The decrease is caused by the removal of tungsten oxide. This assumption is supported by the observation that WO_{3-x} particles are condensed near the irradiated crystal.

TABLE 1
Fractional Atomic Co-ordinates of Metal Atoms (M = Nb, W) in the Structural Model for $(Nb, W)_{12}O_{32}$

	x	y	z
M1	$\frac{1}{4}$	$\frac{1}{4}$	$\frac{1}{2}$
M2	0.071	0.1454	$\frac{1}{2}$
M3	0.071	0.355	$\frac{1}{2}$
M4	0.4295	0.1454	$\frac{1}{2}$
M5	0.4295	0.355	$\frac{1}{2}$
M6	0.244	0.4295	$\frac{1}{2}$

Note. Space group $P4$; $a = 1.73$ nm, $c = 0.39$ nm.

Taking into account the theoretical composition of the new structure, $(Nb, W)_{12}O_{32}$, and that of the starting material, $Nb_7W_{10}O_{47}$, the chemical equation of the transformation can be formulated:

$$Nb_7W_{10}O_{47} \rightarrow Nb_7W_5O_{32} + 5WO_3.$$

Due to the special geometry of the underlying TTB framework, two distinct unit cells are possible for $(Nb, W)_{12}O_{32}$. Although the orientation of the cells is the same, the origins are shifted by $\frac{1}{2}[110]_{TTB}$ with respect to each other (Fig. 8). This geometric relationship corresponds to that of the types of two squares of 2×2 octahedra which are present in the TTB substructure and which are related by an axial glide plane. Twinned microdomains consisting of one of the two unit cell variants appear in Fig. 3. In between these well-ordered microdomains, the PC arrangement is less ordered: single PCs, pairs of diamond-linked PCs, and groups of three PCs appear. Possibly, the disorder is due to the fact that the structure had no time to crystallize perfectly during the short treatment in the electron microscope.

The geometric relation of these cells with the original threefold TTB superstructure is also depicted in Fig. 8. Since the a-axis and the b-axis of the $Nb_8W_9O_{47}$ structure are parallel to the axes of the TTB subcell, whereas those of $(Nb, W)_{12}O_{32}$ are parallel to $\langle 110 \rangle_{TTB}$ directions, the unit cells are rotated by 45° with respect to each other. This relation between the distinct structures can be also seen in Fig. 2a.

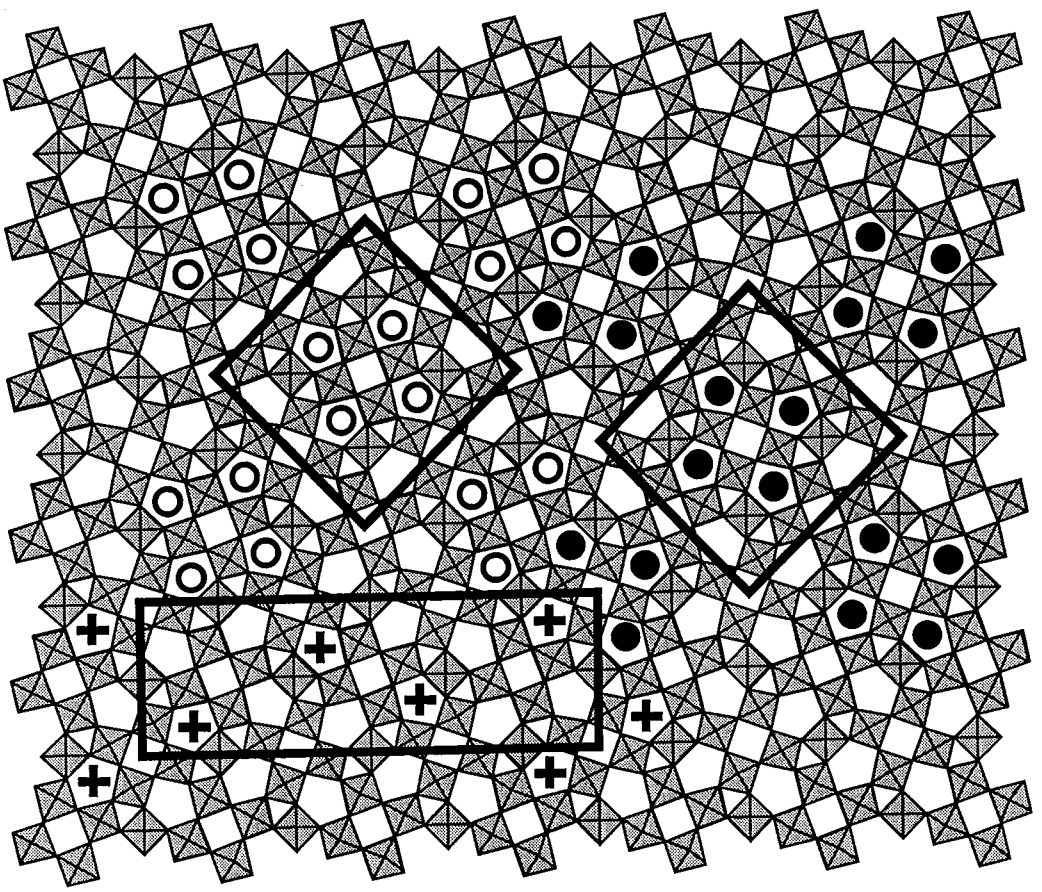

FIG. 8. Octahedral framework of the TTB substructure projected onto the ab-plane. The two variants of the tetragonal unit cell of $(Nb, W)_{12}O_{32}$ ($a = \sqrt{2}a_{TTD}$) are outlined (PCs symbolized as ○ and ●, respectively). For comparison, a unit cell of $Nb_8W_9O_{47}$ ($a = a_{TTB}$, $b = 3a_{TTB}$) is included in this representation (PCs symbolized as +).

For a niobium tungsten oxide, which contains only fully oxidized cations, the formula corresponding to $(Nb, W)_{12}O_{32}$ would be Nb_2WO_8 ($Nb_8W_4O_{32}$). For this particular composition, another niobium tungsten oxide structure is known (16). This structure consists only of PCs and can be prepared by heating mixtures of the binary oxides Nb_2O_5 and WO_3 in the corresponding molar ratio. Although the $O/\sum M$ ratio is the same as for $(Nb, W)_{12}O_{32}$, this structure is apparently not favored as a reaction product when starting with a TTB structure. The TTB framework is extraordinary stable and preserved (at least in large crystal regions) even if drastic structural changes take part, e.g., during the oxidation of not fully oxidized niobium tungsten oxides (12, 13). Thus, it is obviously more advantageous for $Nb_7W_{10}O_{47}$ to accommodate the decreased $O/\sum M$ ratio by forming a new, unusual TTB-superstructure than by reorganizing the octahedral framework.

4. CONCLUSIONS

$(Nb, W)_6O_{16}$ crystallizes in a TTB superstructure which is isostructural with those observed before in $NaNb_5WO_{16}$ (17) as well as in some quaternary niobium oxide fluorides $(K, Na)_xNb_{12}(O,F)_{32}$ (18–20). However, this structure type has been found now for the first time in the ternary system Nb/W/O.

The simultaneous occupation of adjacent PTs observed in $(Nb, W)_{12}O_{32}$ violates the rules (21) found for a systematic and stable arrangement of PCs in the TTB substructure:

1. The PTs adjacent to a PC remain empty.
2. One of two PTs connected to a PC by the diamond link is occupied.

While these rules are strictly obeyed in the $Nb_8W_9O_{47}$ structure, deviating compositions lead to violations of the second rule. Characteristic features of less-ordered niobium tungsten oxides are slabs of diamond linked PCs, which partly accommodate increased $O/\sum M$ ratios by decreasing the amount of occupied tunnels (22). However, these phases are prepared by conventional solid state reactions, whereas the conditions which lead to the formation of $(Nb, W)_{12}O_{32}$ are completely different ones. It seems that the transformation is due to the interaction of the heated gas with the sample, but it does not matter which kind of gas is applied. The atoms in the gas reaction cell are partly ionized by the high-energy electron beam, leading to the formation of a plasma (23). We assume that in a first step of the reaction, a part of the tungsten oxide is etched out of $Nb_7W_{10}O_{47}$, evaporates, and condenses again on the cold carbon foil outside the reaction zone. This process leads to a decreased $O/\sum M$ ratio, which has to be accommodated by the structure. This is performed by changing MO_3 into MO, which means the occupation of more PTs. Thereby, a structural reorganization gives rise to a new superstructure, whereas the stable framework of the TTB structure is preserved. We note that the reaction product is kinetically rather than thermodynamically stable. Also it should be noted that the area of existence (in terms of $O/\sum M$) for conventionally produced TTB-type niobium tungsten oxides is in between 2.765 ($Nb_8W_9O_{47}$) and 2.90. $(Nb, W)_{12}O_{32}$ is the first example with a lower $O/\sum M$ ratio (2.667).

ACKNOWLEDGMENTS

Financial support by the EPSRC (ROPA Grant GR/K36492) and for F.K. by the Swiss National Science Foundation (Grant 20-47171.96) is gratefully acknowledged. We thank Professor Cantor for provision of laboratory facilities and Dr. Sloan for helping with the JEOL 2010 microscope.

REFERENCES

1. R. C. Doole, G. M. Parkinson, J. L. Hutchison, M. J. Goringe, and P. J. F. Harris, *JEOL News* **30E,** 30 (1992); R. C. Doole, G. M. Parkinson, and J. M. Stead, *Inst. Phys. Conf. Series* **118,** 157 (1991).
2. M. J. Sayagués and J. L. Hutchison, *J. Solid State Chem.* **124,** 116 (1996).
3. M. Goringe, A. Rawcliffe, A. Burden, J. Hutchison, and R. Doole, *Faraday Discuss.* **105,** 85 (1996).
4. E. D. Boyes and P. L. Gai, *Ultramicroscopy* **67,** 219 (1997).
5. R. Gruehn, *Natl. Bur. Stand. Spec. Publ.* **364,** 63 (1972).
6. B. G. Hyde and M. O'Keeffe, *Acta Crystallogr. A* **29,** 243 (1973).
7. A. Magnéli, *Arkiv Kemi* **24,** 213 (1949).
8. M. Lundberg, *Chem. Commun. Univ. Stockholm* **XII** (1971).
9. A. W. Sleight, *Acta Chem. Scand.* **20,** 1102 (1966).
10. M. Lundberg, M. Sundberg, and A. Magnéli, *J. Solid State Chem.* **44,** 32 (1982).
11. F. Krumeich, A. Hussain, C. Bartsch, and R. Gruehn, *Z. Anorg. Allg. Chem.* **621,** 799 (1995).
12. F. Krumeich, *J. Solid State Chem.* **119,** 420 (1995).
13. F. Krumeich, C. Bartsch, and R. Gruehn, *J. Solid State Chem.* **120,** 268 (1995).
14. P. Stadelmann, *Ultramicroscopy* **21,** 131 (1987).
15. S. Horiuchi, K. Muramasu, and Y. Matsui, *Acta Crystallogr. A* **34,** 939 (1978).
16. M. Lundberg, *Acta Chem. Scand.* **26,** 2932 (1972).
17. M. Sundberg and B.-O. Marinder, *J. Solid State Chem.* **84,** 23 (1990).
18. M. Lundberg and M. Sundberg, *J. Less-Common Metals* **137,** 163 (1988).
19. M. Lundberg and M. Sundberg, *Chem. Scr.* **28,** 81 (1988).
20. D. X. Li, *J. Solid State Chem.* **73,** 1 (1988).
21. S. Iijima and J. G. Allpress, *Acta Crystallogr. A* **30,** 22 (1974).
22. F. Krumeich, *Acta Cryst. B* **54,** 240 (1998).
23. A. Burden and J. L. Hutchison, *Carbon* **35,** 567 (1997).